Research Article Vol. 4, No. 9 / September 2017 / Optica 1011

Spatial mode-interaction induced single soliton generation in microresonators

Chengying Bao,[1,*] Yi Xuan,[2] Daniel E. Leaird,[1] Stefan Wabnitz,[3] Minghao Qi,[1,2] and Andrew M. Weiner[1,2]

[1]School of Electrical and Computer Engineering, Purdue University, 465 Northwestern Avenue, West Lafayette, Indiana 47907-2035, USA
[2]Birck Nanotechnology Center, Purdue University, 1205 West State Street, West Lafayette, Indiana 47907, USA
[3]Dipartimento di Ingegneria dell'Informazione, Università di Brescia, and INO-CNR, via Branze 38, 25123 Brescia, Italy
*Corresponding author: bao33@purdue.edu

Received 6 June 2017; revised 22 July 2017; accepted 24 July 2017 (Doc. ID 296857); published 22 August 2017

Soliton mode-locking in microresonators enables chip-scale coherent optical frequency comb generation. However, it usually leads to multi-soliton combs with a structured spectrum. Instead, the smooth spectrum of a single soliton is favored for applications. Here, we introduce, experimentally and numerically, a passive mechanism for single temporal soliton formation arising from spatial mode-interaction in microresonators. Deterministic single soliton generation is observed for microresonators with strong mode-interaction in experiments and simulations. Further simulations demonstrate that the soliton number is reduced to one in order to lower the nonlinear loss into mode-interaction induced Cherenkov radiation (CR). Our results give important insights into soliton–CR interaction in cavities.

OCIS codes: (190.5530) Pulse propagation and temporal solitons; (190.4390) Nonlinear optics, integrated optics.

https://doi.org/10.1364/OPTICA.4.001011

1. INTRODUCTION

Kerr combs generated from high-Q microresonators open great prospects for chip-scale optical frequency synthesis [1,2]. Kerr combs are used for numerous applications, including arbitrary optical waveform generation [3], spectroscopy [4], and optical clocks [5]. In those applications, coherent Kerr combs are needed. Soliton mode-locking in the anomalous dispersion regime [6] and dark-pulse mode-locking in the normal-dispersion regime [7] enable repeatable coherent Kerr comb generation. In the normal dispersion regime, the dark-pulse number is usually deterministic [7]. In contrast, in the anomalous dispersion regime, the soliton number is stochastic and usually larger than 1 [8,9]. Multi-soliton combs exhibit a structured spectrum, with large intensity variations between comb lines. For many applications, smooth comb spectra are favored. Hence, the generation of Kerr combs comprising a single soliton is highly desired. By precise control of the laser scanning speed and the stopping wavelength, one can get single solitons. However, the method only works for cavities with weak thermal effects, e.g., MgF_2 microresonators [6]. For microresonators with strong thermal effects, backward tuning of the laser after generating multiple solitons can be used [8]. Using the output comb power as a feedback signal to actively control the pump frequency is an alternative method to achieve a single soliton [10]. Phase or amplitude modulation of the pump [11,12] and simultaneous control of the pump power and frequency [9] can also be used to realize single solitons.

In this paper, we introduce for the first time, to our knowledge, a passive mechanism that leads to single soliton generation in anomalous dispersion microresonators, without the need for any active controls. The method is based on the interaction between spatial modes, which can shift their resonance frequencies and change the local dispersion [13]. This effect was first exploited to initiate comb generation in normal dispersion microresonators [7,13]. For anomalous dispersion microresonators, mode-interaction causes abrupt jumps on the soliton spectrum [14], which originate from the emission of a dispersive wave, also termed as Cherenkov radiation (CR), from the solitons [15,16]. This radiation is usually thought to be detrimental to soliton generation [14]. However, it has been shown that this radiation may be exploited to increase the stability of the soliton repetition rate [17]. Mode-interactions may also stabilize multiple pulses into regularly spaced soliton crystals [18]. More recently, it has been shown both theoretically and experimentally (in fiber cavities) that oscillating tails arising from the beating between the mode-interaction-induced CR and the pump provide local intensity peaks that can trap solitons, thus bringing solitons to regular positions [19,20]. Here, we show that a mode-interaction of appropriate strength can induce single soliton generation in microresonators. By testing soliton generation in two silicon-nitride (SiN) microresonators with the same cross-sectional geometry but different mode-interaction strengths, we observe deterministic single soliton generation in the microresonator with strong mode-interaction, while multi-solitons are generated stochastically in the other microresonator. Numerical simulations based on the Lugiato–Lefever equation (LLE) [21,22] reproduce the single soliton generation induced by mode-interaction. Our work

reveals that, in a dissipative cavity, the CR (induced by mode-interaction in our devices) emitted from solitons has far wider consequences than in a conservative fiber [23]. In an optical fiber, weak CR only provides a perturbation to soliton dynamics [23], whereas in a cavity, weak CR generation may greatly affect the existence of solitons. Beyond microresonators, the revealed importance of CR–soliton interaction in cavities could also affect the pulse dynamics in mode-locked lasers, where resonant radiation widely exists [24].

2. OBSERVATION OF DETERMINISTIC SINGLE SOLITON GENERATION

Solitons are generated in two similar SiN microresonators (Device 1 and Device 2). The two microresonators have the same radius (100 μm) and geometry (800 nm × 2000 nm). The loaded (intrinsic) Q-factors are $2.4 \times 10^6 (3.0 \times 10^6)$ for Device 1 and $1.4 \times 10^6 (4.5 \times 10^6)$ for Device 2, respectively. The coupling coefficient of Device 2 is about 6 times that of Device 1, due to its narrower waveguide-microresonator gap (300 nm compared with 500 nm). We first characterize the resonance frequencies of the two microresonators by linear transmission spectroscopy, with the laser frequency calibrated by a high-precision wavemeter.

The resonance frequency (ν_m) for mode m can be written as $\nu_m = \nu_0 + md_1 + d_2 m^2/2$, where ν_0 is the frequency of the pumped mode (mode $m = 0$), d_1 is the free spectral range (FSR), and d_2 is the group velocity dispersion coefficient. We plot the relative resonance frequencies, i.e., $\nu_m - \nu_0 - md_1$ and their quadratic fits in Fig. 1. The resonance frequency can be shifted by mode-interaction; the magnitude of the shift depends on the coupling strength between the interacting modes and the difference in their resonant frequencies (Supplement 1, Section 4) [13,25]. The two devices have similar FSR and dispersion due to the similar design. Furthermore, localized perturbations to the resonance frequency curves associated with mode-interactions are located around the wavelengths 1526–1528 nm in both devices. However, due to inevitable fabrication differences and the uncontrolled nature of the mode-interactions, arising (for example) from nanoscale roughness, Device 1 is found to have much stronger mode-interaction strength than Device 2. The resonance frequency is shifted by 3.8 GHz for the most strongly perturbed mode for Device 1, whereas the maximum frequency shift for Device 2 is only 0.3 GHz.

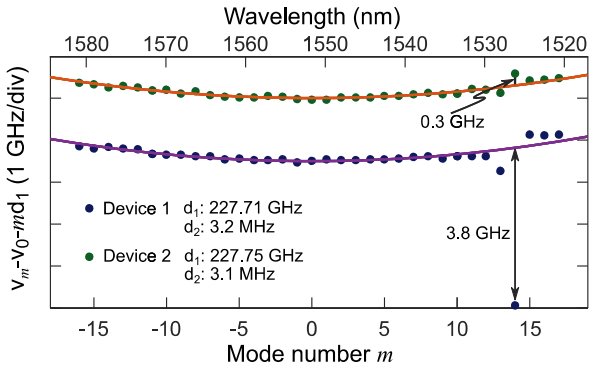

Fig. 1. Measured relative cavity resonance frequencies (circles) of the two devices and their quadratic fits (lines). There is a strong mode-interaction perturbed resonance shift for Device 1, while this shift is much weaker for Device 2. The resonance frequencies of Device 1, 2 are shifted away from each other for clarity.

The difference in mode-interaction strength leads to distinct soliton generation dynamics in these two devices. Only a single soliton is supported in Device 1. To show that, we scan the pump laser across the resonance to map out the soliton step. In 40 scans, we find that the converted comb power traces (output at the through-port after blocking the pump by a notch filter) all exhibit a single soliton step [Fig. 2(a)]. To characterize the single soliton Kerr comb, we stabilize the soliton in Device 1 by abruptly backward tuning the laser after detecting the soliton step [26]. The resulting smooth spectrum indicates single soliton operation, Fig. 2(b). The strong spike (11 dB stronger than the sech^2 fit) on the spectrum at the mode-interaction region is indicative of strong mode-interaction in Device 1, consistent with our linear transmission measurement in Fig. 1. In contrast, the single soliton step only occurs once in 40 scans in Device 2 (Supplement 1, Section 1). Furthermore, multi-soliton combs can be generated in Device 2 following the direct soliton generation method [27]. A representative multiple soliton spectrum is shown in Fig. 2(c). The spectrum is highly structured, and there is no clearly discernible spike at the mode-interaction region (1526–1528 nm). To compare the spectral features of the single soliton state in the two devices, we obtained a single soliton in Device 2 by slowly backward tuning the laser after the soliton is stabilized [8]. Note that the backward tuning of the laser in Device 2 is used for soliton number control, whereas it is used for soliton stabilization in Device 1. The single soliton spectrum in Device 2 [Fig. 2(d)] is similar to that of Device 1; however, the spike at the mode-interaction region is now very weak (~2 dB), again consistent with the weak mode-interaction seen in the linear transmission measurement. The similar properties of the two devices except for the strength of mode-interaction suggests that

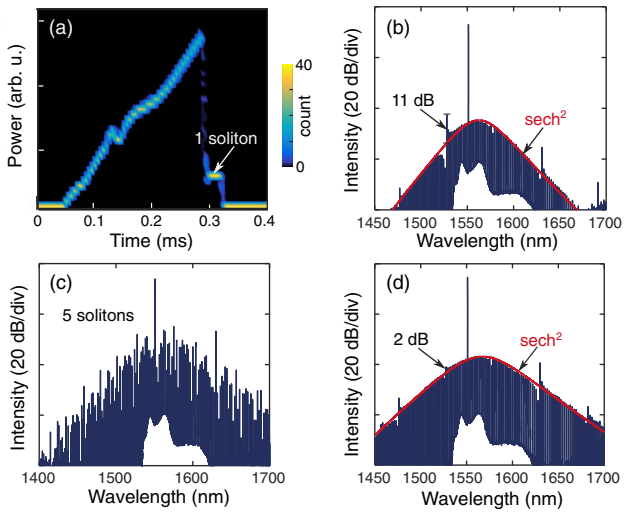

Fig. 2. Soliton generation in two similar devices. (a) Histogram plot of 40 overlaid converted comb power traces for Device 1, when tuning the laser across the resonance. The color density represents the count of trials in which a certain power level occurs during the given time slot. Soliton-step comprising a single soliton is observed in all 40 scans. (b) Single soliton spectrum of Device 1, showing an abrupt jump, 11 dB stronger than sech^2 fit (red lines). (c) Spectrum of the multi-soliton of Device 2. (d) Single soliton spectrum of Device 2 showing a much smaller (2 dB) jump at the mode-interaction region.

mode-interaction could be responsible for the distinct soliton generation dynamics.

Note that there is another spike around 1631 nm (outside the range of our linear transmission measurement) in both devices. However, because it is in the wings of the spectrum, its absolute intensity is much weaker than the one around 1528 nm in Fig. 2(b). Hence, it has a smaller effect on soliton generation dynamics (Supplement 1, Section 2).

3. NUMERICAL SIMULATIONS ON SOLITON DYNAMICS PERTURBED BY MODE-INTERACTION

To further unveil the role of mode-interactions in single soliton generation, we use numerical simulations based on the generalized LLE to look into the soliton generation dynamics [21,22,28]. The generalized LLE can be written as

$$\left(t_R\frac{\partial}{\partial t}+\frac{\alpha+\kappa}{2}+i\frac{\beta_2 L}{2}\frac{\partial^2}{\partial\tau^2}+i\delta\right)E-\sqrt{\kappa}E_{\text{in}} - i\gamma L\left(E\int_{-\infty}^{+\infty}R(\tau')|E(t,\tau-\tau')|^2\mathrm{d}\tau'\right)=0, \quad (1)$$

where E, L, t_R, β_2, γ, α, κ, δ, E_{in} are the envelope of the intracavity field, cavity length, round-trip time, group-velocity dispersion, nonlinear coefficient, intrinsic and coupling loss, pump phase detuning, and pump amplitude, respectively; $R(\tau)$ is the nonlinear response of SiN, including the instantaneous electronic and delayed Raman response (see Ref. [28] for its calculation method). Mode-interaction is included by adding a phase shift $\phi(\omega)$ per round trip to the perturbed modes (ω is the frequency relative to the pump) [7]. We write the mode-interaction phase term as $\phi(\omega)=a/(\omega-\omega_1)$ [14]. Thus, mode-interaction only affects modes around ω_1 and vanishes rapidly due to the discrete feature of ω and the large FSR; a reflects the strength of mode-interaction. To mimic the experimentally used devices, we choose $\omega_1=2\pi\times13.8/t_R$, and other parameters as $t_R=4.4$ ps, $L=628$ μm, $\alpha=2.4\times10^{-3}$, $\kappa=3.75\times10^{-4}$, $\beta_2=-81ps^2/km$, $\gamma=0.9\,(Wm)^{-1}$, and $|E_{\text{in}}|^2=0.22W$. Simulations start from noise and the detuning δ is tuned linearly from −0.0041 to 0.0165 in 120 ns and held constant at 0.0165 for another 120 ns to trigger the soliton generation. Depending on mode-interaction strength (a), simulations show distinct results.

We first choose a relatively weak mode-interaction strength ($a_0=-2\pi\times0.6$ GHz). We find that the weak mode-interaction does not affect the soliton number significantly, and multi-solitons can still be accessed. For instance, a simulated evolution of the temporal field E is shown in Fig. 3(a), where we can see that 4 solitons are generated after the chaotic state. To have a better idea of the generated soliton number under this weak mode-interaction, we run 50 laser scans (starting from different noise conditions) and record the intracavity average power change. The histogram of the 50 overlaid recorded power traces is shown in Fig. 3(b). The final soliton number is essentially random, similar to the case without mode-interaction [9].

Distinct from the weak mode-interaction case, deterministic single soliton formation is observed in simulations with a stronger mode-interaction ($a_1=-2\pi\times3.8$ GHz). A single soliton is generated by tuning the pump laser in the same way. The simulated spectrum of the single soliton is shown in Fig. 3(c), which also has a strong spike at the mode-interaction region, in excellent agreement with the experimental spectrum. In the time domain, the beat between this spike and the pump line contributes to an oscillating tail with a period of $\tau_{\text{osc}}=0.34$ ps [Fig. 3(d)]. An example of the simulated generation dynamics of the single soliton is depicted in Fig. 3(e). Only one soliton is generated from the chaotic waveform. The histogram of the overlaid simulated power changes in 50 laser scans further shows the deterministic generation of a single soliton [Fig. 3(f)].

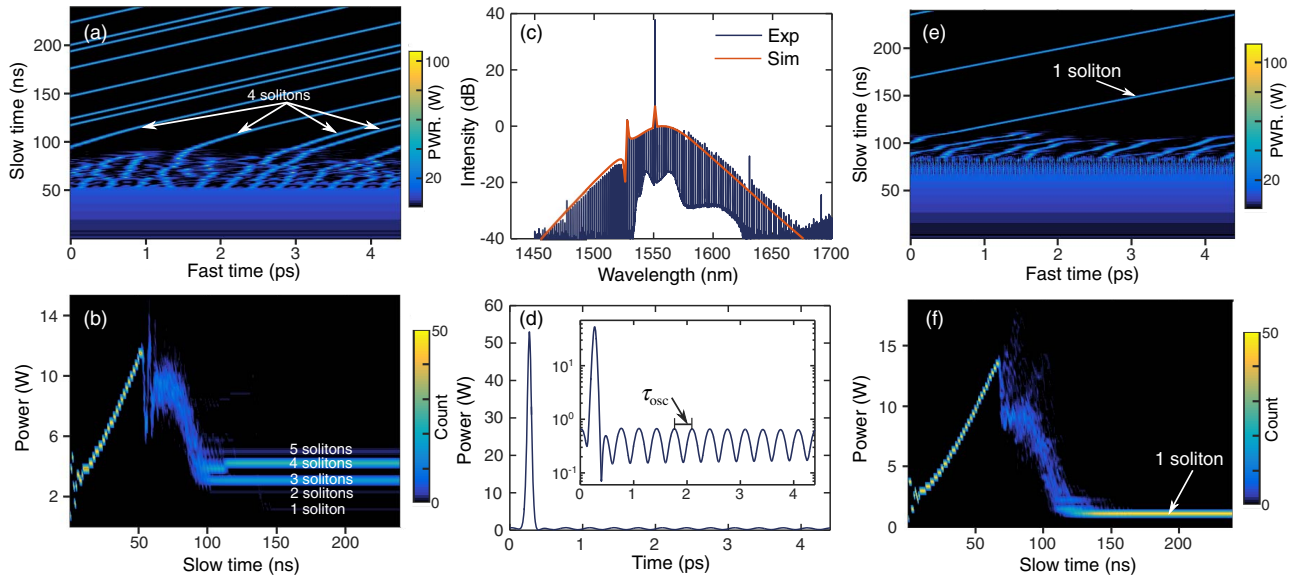

Fig. 3. Numerical simulations on single soliton generation from mode-interaction. (a) An example of the soliton generation dynamics under weak mode-interaction. Four solitons are generated from the chaotic state. (b) Histogram of 50 overlaid intracavity power traces during the laser scan under weak mode-interaction. The number of the generated soliton is stochastic, with 3 and 4 being the dominant cases. (c) Comparison of the simulated and experimental spectrum of the single soliton under a strong mode-interaction, (d) the corresponding temporal soliton; the logarithmic plot in the inset clearly shows an oscillating tail. (e) An example of generation dynamics of a single soliton under strong mode-interaction; (f) the corresponding histogram of 50 overlaid power traces during the laser scan, showing deterministic single soliton generation.

From Figs. 2 and 3, we can see that the deterministic single soliton generation is accompanied by strong mode-interaction-induced CR. The CR generation acts as a nonlinear loss mechanism for the solitons [29], which contributes in an important way to the observed single soliton generation. Simulations show that the peak power and energy of the generated solitons are reduced when mode-interaction is turned on, which provides evidence of the proposed loss mechanism (see Supplement 1, Section 3). To illustrate this premise, we write a single soliton field (the pump related cw background excluded) as $E_1(\tau)$ and its spectrum as $S_1(\omega)$. The spectrum has CR due to mode-interaction perturbation at the frequency ω_{CR}. When there are n solitons located at different time points τ_j, the associated spectrum $S_n(\omega)$ can be written as

$$S_n(\omega) = \mathrm{F.T.}\left\{\sum_{j=1}^{j=n} E_1(\tau-\tau_j)\right\} = S_1(\omega)e^{i\omega\tau_1}\sum_{j=1}^{j=n} e^{i\omega(\tau_j-\tau_1)}, \quad (2)$$

where F.T. stands for Fourier transform. Since multiple solitons share the same cw background and their relative phase to the background should be the same [22], we assume the phase of the multiple solitons to be the same. It was shown recently that mode-interactions can bring multiple solitons into a regular temporal spacing that satisfies $\omega_{\mathrm{CR}}(\tau_j-\tau_1) = 2k\pi$ (k is an integer) [19,20]. Thus, the spectrum of multiple solitons evaluated at the CR frequency is n^2 that of a single soliton, i.e., $|S_n(\omega_{\mathrm{CR}})|^2 = n^2|S_1(\omega_{\mathrm{CR}})|^2$. Hence, the multi-soliton states experience large CR-induced nonlinear loss, which leads to their annihilation. Consequently, over a certain range of mode-interaction strength, a single soliton state is generated, which minimizes CR-induced nonlinear loss in the presence of mode-interaction.

To support this hypothesis, we seed the simulation with two solitons (soliton peak power determined by the analytical solution [22] excluding soliton background and CR) separated by $0.5t_R$, equal to 2.2 ps ($\sim 6.5\tau_{\mathrm{osc}}$), with detuning $\delta = 0.0165$ and mode-interaction strength $a = -2\pi \times 3.8$ GHz. We depict the soliton evolution, soliton separation, and CR power in Figs. 4(a)–4(c), respectively. Upon propagation, the CR power gradually grows, and the soliton separation moves to $\sim 7\tau_{\mathrm{osc}}$, consistent with Refs. [19,20]. The strong CR nonlinear loss destabilizes the solitons, which start to breathe [shaded box in Fig. 4(a)]. Associated with this breathing, the soliton separation and CR power also change quasi-periodically. The oscillation rate of CR power is approximately twice that of the soliton separation, since $|S_n(\omega_{\mathrm{CR}})|^2$ is proportional to $\cos(\omega_{\mathrm{CR}}(\tau_2-\tau_1))$ and $\omega_{\mathrm{CR}}(\tau_2-\tau_1)$ crosses $2k\pi$ two times per oscillation of the soliton separation. To regain stability, one of the solitons annihilates, which lowers the power in the CR. The maximum transient CR power (P_t) in Fig. 4(c) is 3.2 times the steady single soliton CR power (P_s), close to the expected 4 times. The deviation can be attributed to the spectral recoiling of the CR, which reduces the CR [29]. Moreover, based on the above interpretation, there should be an upper limit for the soliton number in the presence of mode-interaction.

To test the existence of this limit, we simulate the soliton dynamics under moderate mode-interaction strength. In particular, we reduce the mode-interaction strength to $a = -2\pi \times 2.7$ GHz and tune the laser as in Figs. 3(b) and 3(f) to induce solitons. The recorded power change in 50 scans starting from different noise seeds is shown in Fig. 4(d); the final comb state always consists of 2 solitons, and a larger soliton number is not accessed. To verify

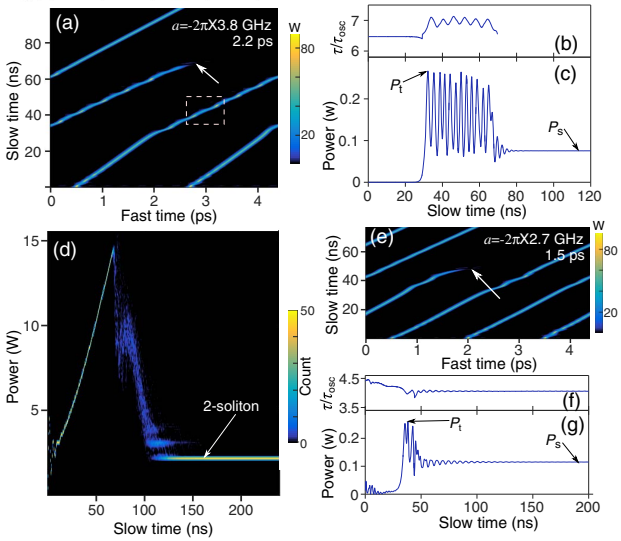

Fig. 4. Cherenkov radiation and single soliton generation. (a) Single soliton generation under $a = -2\pi \times 3.8$ GHz when seeding with 2 solitons separated by 2.2 ps. One of the soliton annihilates in propagation (see the arrow). Prior to the annihilation, solitons breathe, as shown by the dashed box. (b) Change of the separation between the 2 solitons in propagation. (c) Change of CR power; the CR power reaches a maximum transient power (P_t), which is 3.2 times the steady CR power (P_s) when a single soliton is formed. (d) Simulated histogram of 50 overlaid power traces when tuning the laser to induce solitons under $a = -2\pi \times 2.7$ GHz. 2 solitons are always obtained in the 50 scans. (e) Soliton evolution under $a = -2\pi \times 2.7$ GHz when seeding with 3 solitons separated by 1.5 ps; one of the solitons annihilate (see the arrow), generating 2 solitons. (f) Change of the soliton separation between the 2nd and 3rd soliton. (g) Change of the CR power; CR reaches a P_t, 2.18 times of P_s.

that soliton numbers ≥ 3 are unstable for $a = -2\pi \times 2.7$ GHz, we inject three solitons separated by 1.5 ps (equal to $\sim 0.33t_R$ and $\sim 4.5\tau_{\mathrm{osc}}$) into the simulation at $\delta = 0.0165$. In the simulation, one of the solitons is observed to annihilate upon propagation [Fig. 4(e)]. The separation between the 2nd and 3rd solitons is found to be reduced from $\sim 4.5\tau_{\mathrm{osc}}$ to $\sim 4\tau_{\mathrm{osc}}$ [Fig. 4(f)]. Furthermore, the CR power increases to a high value when three solitons exist and are regularly spaced. To mitigate this high nonlinear loss induced instability [see the variations in Figs. 4(e)–4(g)], the soliton number drops down to 2, after which the remaining solitons regain stability. In this case, P_t is $2.18P_s$, also close to the expected value of 9/4. Further simulations suggesting that solitons can be removed one by one by sequentially increasing the mode-interaction strength (see Supplement 1, Section 4). Our picture can also be used to elucidate the fact that a soliton state is prohibited by an even stronger mode-interaction [14]. The higher loss to CR then causes even a single soliton to annihilate because the pump power is insufficient to sustain a soliton [22].

4. CONCLUSION

In conclusion, we have revealed a passive mechanism arising from spatial mode-interaction that can result in deterministic single soliton generation in microresonators. Simulations suggest that the soliton number tends to reduce to 1 in order to avoid a high nonlinear loss into the CR. Our results provide evidence that the interplay between CR and solitons in cavities can greatly

modify the interactions between solitons, impacting the stability of multi-soliton states. The strength of the mode-interaction and its location with respect to the pump frequency may be tuned in a programmable way by using the dual-ring structure of [30], which potentially enables exploitation of the deterministic single soliton approach revealed here without the need to select specific devices.

Funding. Defense Advanced Research Projects Agency (DARPA) (W31P40-13-1-0018); Air Force Office of Scientific Research (AFOSR) (FA9550-15-1-0211); National Science Foundation (NSF) (ECCS-1509578); Ministero dell'Istruzione, dell'Università e della Ricerca (MIUR) (PRIN 2015KEZNYM).

See Supplement 1 for supporting content.

REFERENCES

1. P. Del'Haye, A. Schliesser, O. Arcizet, T. Wilken, R. Holzwarth, and T. J. Kippenberg, "Optical frequency comb generation from a monolithic microresonator," Nature **450**, 1214–1217 (2007).
2. T. Kippenberg, R. Holzwarth, and S. Diddams, "Microresonator-based optical frequency combs," Science **332**, 555–559 (2011).
3. F. Ferdous, H. Miao, D. E. Leaird, K. Srinivasan, J. Wang, L. Chen, L. T. Varghese, and A. M. Weiner, "Spectral line-by-line pulse shaping of on-chip microresonator frequency combs," Nat. Photonics **5**, 770–776 (2011).
4. M.-G. Suh, Q.-F. Yang, K. Y. Yang, X. Yi, and K. J. Vahala, "Microresonator soliton dual-comb spectroscopy," Science **354**, 600–603 (2016).
5. S. B. Papp, K. Beha, P. Del'Haye, F. Quinlan, H. Lee, K. J. Vahala, and S. A. Diddams, "Microresonator frequency comb optical clock," Optica **1**, 10–14 (2014).
6. T. Herr, V. Brasch, J. Jost, C. Wang, N. Kondratiev, M. Gorodetsky, and T. Kippenberg, "Temporal solitons in optical microresonators," Nat. Photonics **8**, 145–152 (2014).
7. X. Xue, Y. Xuan, Y. Liu, P.-H. Wang, S. Chen, J. Wang, D. E. Leaird, M. Qi, and A. M. Weiner, "Mode-locked dark pulse Kerr combs in normal-dispersion microresonators," Nat. Photonics **9**, 594–600 (2015).
8. H. Guo, M. Karpov, E. Lucas, A. Kordts, M. H. P. Pfeiffer, V. Brasch, G. Lihachev, V. E. Lobanov, M. L. Gorodetsky, and T. J. Kippenberg, "Universal dynamics and deterministic switching of dissipative Kerr solitons in optical microresonators," Nat. Phys. **13**, 94–102 (2017).
9. J. A. Jaramillo-Villegas, X. Xue, P.-H. Wang, D. E. Leaird, and A. M. Weiner, "Deterministic single soliton generation and compression in microring resonators avoiding the chaotic region," Opt. Express **23**, 9618–9626 (2015).
10. X. Yi, Q.-F. Yang, K. Youl, and K. Vahala, "Active capture and stabilization of temporal solitons in microresonators," Opt. Lett. **41**, 2037–2040 (2016).
11. V. Lobanov, G. Lihachev, N. Pavlov, A. Cherenkov, T. Kippenberg, and M. Gorodetsky, "Harmonization of chaos into a soliton in Kerr frequency combs," Opt. Express **24**, 27382–27394 (2016).
12. H. Taheri, A. A. Eftekhar, K. Wiesenfeld, and A. Adibi, "Soliton formation in whispering-gallery-mode resonators via input phase modulation," IEEE Photon. J. **7**, 1–9 (2015).
13. Y. Liu, Y. Xuan, X. Xue, P.-H. Wang, S. Chen, A. J. Metcalf, J. Wang, D. E. Leaird, M. Qi, and A. M. Weiner, "Investigation of mode coupling in normal-dispersion silicon nitride microresonators for Kerr frequency comb generation," Optica **1**, 137–144 (2014).
14. T. Herr, V. Brasch, J. D. Jost, I. Mirgorodskiy, G. Lihachev, M. L. Gorodetsky, and T. J. Kippenberg, "Mode spectrum and temporal soliton formation in optical microresonators," Phys. Rev. Lett. **113**, 123901 (2014).
15. A. B. Matsko, W. Liang, A. A. Savchenkov, D. Eliyahu, and L. Maleki, "Optical Cherenkov radiation in overmoded microresonators," Opt. Lett. **41**, 2907–2910 (2016).
16. Q.-F. Yang, X. Yi, K. Y. Yang, and K. Vahala, "Spatial-mode-interaction-induced dispersive waves and their active tuning in microresonators," Optica **3**, 1132–1135 (2016).
17. X. Yi, Q.-F. Yang, X. Zhang, K. Y. Yang, X. Li, and K. Vahala, "Single-mode dispersive waves and soliton microcomb dynamics," Nat. Commun. **8**, 14869 (2017).
18. D. C. Cole, E. S. Lamb, P. Del'Haye, S. A. Diddams, and S. B. Papp, "Soliton crystals in Kerr resonators," arXiv:1610.00080 (2016).
19. Y. Wang, F. Leo, J. Fatome, M. Erkintalo, S. G. Murdoch, and S. Coen, "Universal mechanism for the binding of temporal cavity solitons," Optica **4**, 855–863 (2017).
20. H. Taheri, A. B. Matsko, and L. Maleki, "Optical lattice trap for Kerr solitons," Eur. Phys. J. D **71**, 153 (2017).
21. S. Coen, H. G. Randle, T. Sylvestre, and M. Erkintalo, "Modeling of octave-spanning Kerr frequency combs using a generalized mean-field Lugiato-Lefever model," Opt. Lett. **38**, 37–39 (2013).
22. S. Wabnitz, "Suppression of interactions in a phase-locked soliton optical memory," Opt. Lett. **18**, 601–603 (1993).
23. D. V. Skryabin and A. V. Gorbach, "Colloquium: looking at a soliton through the prism of optical supercontinuum," Rev. Mod. Phys. **82**, 1287–1299 (2010).
24. L. Nelson, D. Jones, K. Tamura, H. Haus, and E. Ippen, "Ultrashort-pulse fiber ring lasers," Appl. Phys. B **65**, 277–294 (1997).
25. H. A. Haus and W. Huang, "Coupled-mode theory," Proc. IEEE **79**, 1505–1518 (1991).
26. P.-H. Wang, J. A. Jaramillo-Villegas, Y. Xuan, X. Xue, C. Bao, D. E. Leaird, M. Qi, and A. M. Weiner, "Intracavity characterization of micro-comb generation in the single-soliton regime," Opt. Express **24**, 10890–10897 (2016).
27. C. Bao, Y. Xuan, J. A. Jaramillo-Villegas, D. E. Leaird, and A. M. Weiner, "Direct soliton generation in microresonators," Opt. Lett. **42**, 2519–2522 (2017).
28. C. Bao, J. A. Jaramillo-Villegas, Y. Xuan, D. E. Leaird, M. Qi, and A. M. Weiner, "Observation of Fermi-Pasta-Ulam recurrence induced by breather solitons in an optical microresonator," Phys. Rev. Lett. **117**, 163901 (2016).
29. N. Akhmediev and M. Karlsson, "Cherenkov radiation emitted by solitons in optical fibers," Phys. Rev. A **51**, 2602–2607 (1995).
30. X. Xue, Y. Xuan, P. H. Wang, Y. Liu, D. E. Leaird, M. Qi, and A. M. Weiner, "Normal-dispersion microcombs enabled by controllable mode interactions," Laser Photon. Rev. **9**, L23–L28 (2015).